Materials Science & Engineering A 561 (2013) 245–251

Contents lists available at SciVerse ScienceDirect

Materials Science & Engineering A

journal homepage: www.elsevier.com/locate/msea

Effects of V on phase formation and plasticity improvement in Cu–Zr–Al glassy alloys

C.N. Kuo [a], J.C. Huang [a,*], X.H. Du [a], Y.C. Chen [b], X.J. Liu [c], T.G. Nieh [a,d]

[a] Department of Materials and Optoelectronic Science; Center for Nanoscience and Nanotechnology, National Sun Yat-Sen University, Kaohsiung, Taiwan 804, ROC
[b] Department of Logistics Management, Shu-Te University, Kaohsiung, Taiwan 82445, ROC
[c] Department of Materials Science and Engineering, and Research Center of Materials Design and Application, Xiamen University, Xiamen 361005, PR China
[d] Department of Materials Science and Engineering, The University of Tennessee, Knoxville, TN 37996, USA

ARTICLE INFO

Article history:
Received 11 July 2012
Received in revised form
29 October 2012
Accepted 2 November 2012
Available online 10 November 2012

Keywords:
Bulk metallic glass
Microstructure
Compression test

ABSTRACT

Vanadium was alloyed to an amorphous Cu–Zr–Al alloy to induce B2-CuZr phase formation in order to improve plasticity. The vanadium addition was based on the fact that it has a positive heat of mixing with the major constituents in the Cu–Zr–Al alloy, thus could cause liquid phase separation. Microstructural examination showed that V was dissolved in the amorphous matrix and promoted the formation of B2-CuZr precipitates in $(Cu_{47.5}Zr_{47.5}Al_5)_{99}V_1$, improving the plasticity by doubling the fracture strain to 9.4%. However, when V content is more than 3 at%, brittle intermetallic compound phases ($V+Al_{23}V_4$) form and degrade the plasticity. The role of vanadium on plasticity improvement was discussed in the frame of shear band multiplication, energy dissipation during shear banding, twinning/phase-transformation of the B2-CuZr particles during deformation, and deformation induced B2-CuZr particle coarsening. An energy-balance analysis based on deformation-induced B2 particle coarsening produced an interfacial energy of 0.293 J/m^2 for the B2 particle–glassy matrix interface. The result appears to indirectly support the previous idea that plasticity in $Cu_{47.5}Zr_{47.5}Al_5$ is caused by dynamic coarsening of the B2-CuZr particles.

1. Introduction

Bulk metallic glasses (BMGs) have attracted large attention because of their unique properties, such as high strength, large elastic limit, good shaping properties in the viscous state, and reasonable corrosion resistance [1–4]. However, metallic glasses are also known for being extremely brittle, failing in a catastrophic manner, as a result of the formation of localized shear bands [5,6]. In tension, metallic glasses can be stretched elastically to typically about 2% of strain, followed by drastic shear-off fracture [6]. In compression, highly localized shear along the principal shear plane dominates and the materials usually exhibit shear softening and insufficient plastic strain [7–9]. Composite approaches, both extrinsic [10] and intrinsic [11], have been used to subdue the shear band propagation but with limited success.

Recently, it was demonstrated that tensile plasticity of BMGs could be enhanced by introducing micron or nano-scale into the amorphous matrix [12,13]. For example, Pauly et al. [12] showed that the presence of B2-CuZr nanoparticles in a $Cu_{47.5}Zr_{47.5}Al_5$ alloy could apparently improve its tensile plasticity. The B2-CuZr nanoparticles, 2–5 nm in the as-cast condition, were able to twin, phase-transform, and coarsen (to 10–50 nm) under deformation. These deformation processes could prevent plastic instability and dissipate energy, thereby improved the ductility. Wu et al. [13] also demonstrated that a minor 0.5 at% addition of Co in the $Zr_{48}Cu_{47.5}Al_4Co_{0.5}$ alloy could further improve the tensile ductility, due to much larger B2-CuZr spherical particles up to 100 μm. In this Co-containing alloy, the strain hardening rate was enhanced and plastic instability was suppressed due to a B2-CuZr to B19′-ZrCu martensitic transformation, similar to transformation-induced plasticity (TRIP) steels. It is noted that, in the Cu–Zr–Al–Co system, the mixing enthalpy of binary Cu–Co is positive, but other binary constituents are all negative.

In careful examination of the papers by Pauly et al. [12] and Wu et al. [13], we note that the size of the B2 phase seems to impose some effects on the twining or martensitic transformation. The B2 particles smaller than about 25 nm in $Cu_{47.5}Zr_{47.5}Al_5$ [12] or about 80 nm in $Zr_{48}Cu_{47.5}Al_4Co_{0.5}$ [13] were not seen to exhibit twining or martensitic transformation. Thus, it is of interest in exploring if the alloys with abundant B2 particles less than 10 nm would also contribute twining or martensitic transformation induced plasticity.

Vanadium has similar thermodynamic features as Co with respect to the Cu–Zr–Al system. Specifically, the mixing enthalpy

* Corresponding author. Tel.: +886 7 5252000x4063; fax: +886 7 5254099.
E-mail address: jacobc@mail.nsysu.edu.tw (J.C. Huang).

0921-5093/$ - see front matter © 2012 Elsevier B.V. All rights reserved.
http://dx.doi.org/10.1016/j.msea.2012.11.011

of binary Cu–V is also positive (+5 kJ/mol) [14] but the mixing enthalpy of other binary constituents are all negative [14], as listed in Table 1. Furthermore, minor addition of vanadium can change the crystallization mode to encourage the precipitation of Cu–Zr phase of the samples, leading to change of mechanical properties. However, the glass forming ability would decrease with further increasing V content [15]. Based on these, an enhancement of mechanical properties by a minor addition of V is expected. Furthermore, since the heat of mixing between the two major constituents in this system, Cu and Zr, is more negative than that between other elemental combinations, more B2-CuZr particles are expected when V is added to displace Cu from the amorphous matrix. By using our mini-suction furnace, the B2 particles are all smaller than 10 nm in the as-cast condition. It is suitable to examine the microstructure and mechanical response, particularly the possible occurrence of twining or martensitic transformation associated with such fine particles.

Table 1
Relationship between the heats of mixing among the component elements in the Cu–V–Zr–Al alloy system (unit: kJ/mol) [14].

	Cu	V	Zr	Al
Cu		+5	-23	-1
V	+5		-4	-16
Zr	-23	-4		-44
Al	-1	-16	-44	

2. Experimental

There are apparent miscibility gap in the binary phase diagram of both Cu–Co and Cu–V systems, as shown in Fig. 1(a) [16] and Fig. 1(b) [17]. To further examine the thermodynamic features with V addition in Cu–Zr–Al system, the vertical section of the Cu–V–Zr phase diagram (Fig. 1(c)) has been simulated and it shows that there exists a miscibility gap in the V-rich compositions. The result suggests the possibility of forming a phase-separated BMGC upon solidification. Our experience indeed indicates that the casting of Cu–Zr–V becomes more difficult at a higher V content. Thus, low V-containing samples were chosen for the current study.

Rods with compositions of $(Cu_{47.5}Zr_{47.5}Al_5)_{100-x}V_x$ (x=0, 1, 2, 3, 5, and 10) (in at%) and 2 mm in diameter were prepared by suction casting using BÜHLER Mini Arc Melting System MAM-1. The ingots were initially prepared by arc melting under a purified argon atmosphere. After homogenization, the melt was in-situ sucked into a cylindrical-shaped cavities Cu mold cooled by water. Since the cylindrical cavity in this mini furnace is smaller than most larger-scale injection or suction furnaces, the melt would be more rigorously stirred and cooled. The precipitated crystalline B2 phase tends to be much smaller, typically in the range of 3–5 nm. The amorphous nature of the as-cast alloy rods was verified using several analytical systems, including Siemens D5000 X-ray Diffractometer (XRD) with Cu-K_α radiation, SETARAM DSC 131 differential scanning calorimeter (DSC) at a constant heating rate of 0.33 K/s (or 20 K/min), and the JEOL

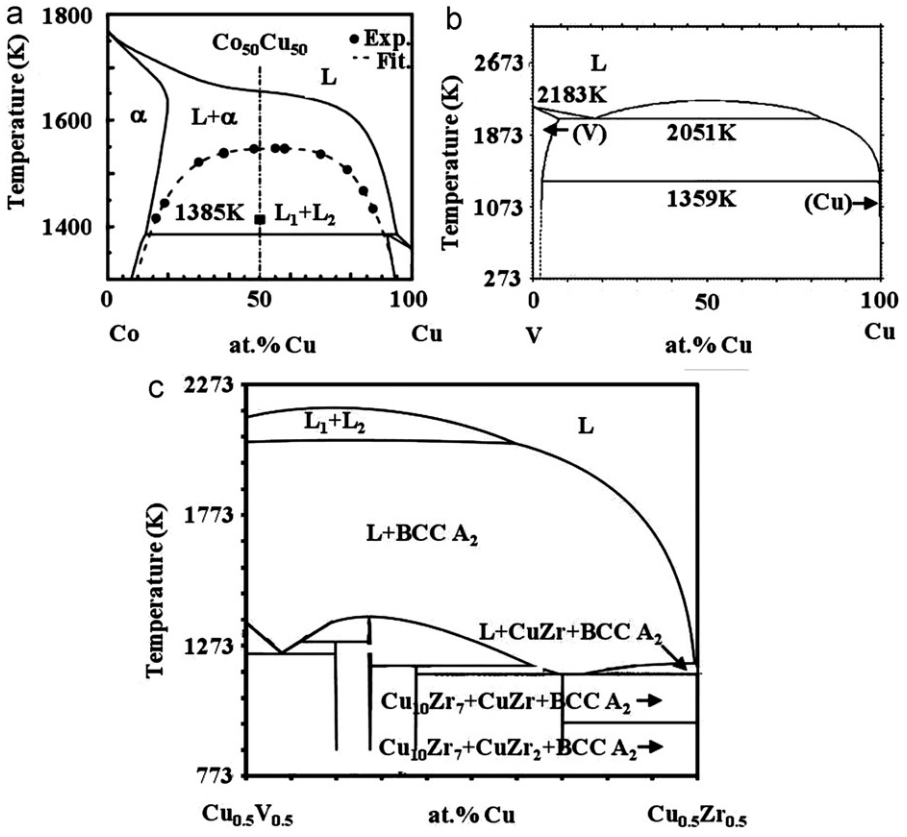

Fig. 1. The related phase diagrams: (a) the Co–Cu binary [16], (b) the V–Cu binary [17] and (c) the simulated $Cu_{50}V_{50}Zr_0$ to $Cu_{50}V_0Zr_{50}$ section.

JSM-6330 scanning electron microscopy (SEM) with energy dispersive spectrometry (EDS).

Compressive samples with a standard aspect ratio of 2 were subsequently prepared from the as-cast Cu-based alloy rods. Two end surfaces of the samples were polished to produce parallel surfaces, which are perpendicular to the longitudinal axis. Room-temperature compression tests were carried out using the Instron 5582 universal testing machine at an initial strain rate of $1\times10^{-4}\,s^{-1}$. To accurately measure the displacement, Instron 2601 Linear Variable Differential Transducer (LVDT) was mounted on test specimens. Thermomechanical analysis (TMA) was employed to measure the viscosity of the BMG samples from room temperature to 875 K, especially at temperatures near and within the supercooled liquid region. The measurements were conducted at a heating rate of 10 K/min. A Tecnai Field-Emission transmission electron microscopy (TEM), operated at 200 kV, was used to characterize the microstructures and the composition of precipitates and phases. TEM foil samples were prepared by focus ion beam (FIB) milling. The volume fraction of the B2 particles was measured by [18]

$$f=\left(\frac{-4\pi r}{2\pi r+8t}\right)\ln(1-A), \quad (1)$$

where r is the average diameters of the B2 particle, t is the TEM foil thickness ($\sim$50 nm), and A is the projected area fraction of the particles.

3. Results

3.1. Microstructure

X-ray diffraction (XRD) patterns obtained from various as-cast $(Cu_{47.5}Zr_{47.5}Al_5)_{100-x}V_x$ (x=0, 1, 2, 3, 5, and 10) (in at%) samples are presented in Fig. 2. The patterns from $Cu_{47.5}Zr_{47.5}Al_5$ and $(Cu_{47.5}Zr_{47.5}Al_5)_{99}V_1$ samples are noted to consist of a single broad diffraction peak, indicating the amorphous structure. The broad diffuse hump locates between 35° and 45° and there is no apparent crystalline peak. By contrast, both $(Cu_{47.5}Zr_{47.5}Al_5)_{97}V_3$ and $(Cu_{47.5}Zr_{47.5}Al_5)_{90}V_{10}$ samples reveal the presence of pure V and $Al_{23}V_4$ crystalline peaks over the broad-like diffraction peak. To ensure these samples were not completely crystallized, DSC scans were subsequently conducted. The results (not shown here) reveal the existence of glass transition (T_g) at $\sim$695 K and crystallization (T_x) temperatures at $\sim$740 K in these samples, with a supercooled liquid region, ΔT_x, about 45 K. No apparent variation of T_g, T_x and ΔT_x with the V content was observed, suggesting these high-V containing alloys are composites consisting of V and $Al_{23}V_4$ particles dispersed in an amorphous matrix.

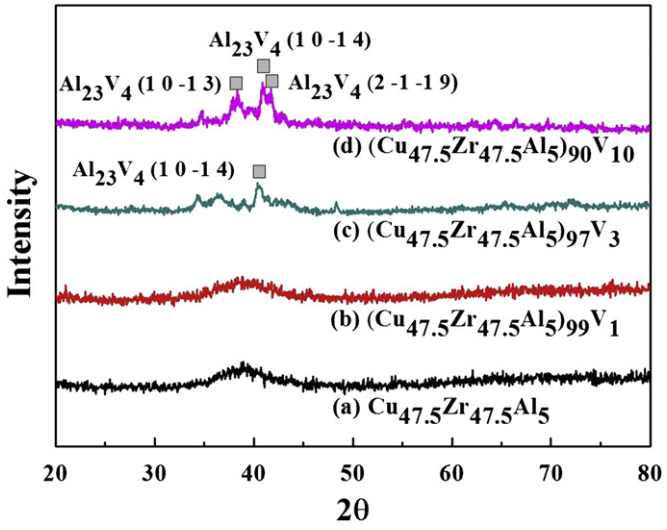

Fig. 2. XRD curves for the four alloys with V contents from 0 to 10 at%.

SEM micrographs (backscattered electron image (BEI)) of the as-cast $Cu_{47.5}Zr_{47.5}Al_5$ and $(Cu_{47.5}Zr_{47.5}Al_5)_{99}V_1$ samples are shown in Figs. 3(a) and (b), respectively. These micrographs are essentially featureless, without any phase contrast, indicating a homogeneous microstructure. By comparison, microstructures of the as-cast $(Cu_{47.5}Zr_{47.5}Al_5)_{97}V_3$ and $(Cu_{47.5}Zr_{47.5}Al_5)_{90}V_{10}$ samples (Figs. 3(c) and (d)) show obvious phase contrast, indicative of the presence of darker crystalline phases in the brighter glassy matrix. Chemical compositions measured by EDS from the two phases confirm that there are some chemical differences between the two phases, especially in the Cu and V content. The results suggest that, in the liquid state, Cu and V might be separated due to a positive heat of mixing between them, as indicated by the calculated phase diagram in Fig. 1(c). During cooling from the liquid state, the two elements partition separately in the solidified phases. Since both binary Cu–Zr and V–Al have a high negative heat of mixing (Table 1), it leads to the formation of the Cu–Zr rich (brighter) and V–Al rich regions (darker) in the solidified product. Based on the XRD and SEM/EDS results, it is concluded that the dark regions in $(Cu_{47.5}Zr_{47.5}Al_5)_{97}V_3$ and $(Cu_{47.5}Zr_{47.5}Al_5)_{90}V_{10}$ are mixtures of V and $Al_{23}V_4$ particles with a size of about 1–2 μm. The volume fractions of these particles are estimated from SEM and TEM and complied in Table 2.

Microstructures of samples were also examined using bright-field and high-resolution TEM. In the as-cast samples, no phase contrast is discernible in the TEM micrographs taken from $Cu_{47.5}Zr_{47.5}Al_5$, but some B2-CuZr particles measuring about 3–5 nm in size were observed in $(Cu_{47.5}Zr_{47.5}Al_5)_{99}V_1$. After deformation, few B2-CuZr phases with crystalline lattice fringes (4–6 nm in size) become apparent in $Cu_{47.5}Zr_{47.5}Al_5$ at high magnifications, as shown in Fig. 4(a). More B2 precipitates were seen in the deformed $(Cu_{47.5}Zr_{47.5}Al_5)_{99}V_1$ specimens, measuring slightly larger to 8–11 nm (Fig. 4(b)). Note that such B2 particles are much finer than those observed previously [12,13]. The volume fractions of the fine B2 phase were also measured using Eq. (1), and the data are included in Table 2.

3.2. Compressive properties

Uniaxial compression tests were conducted on the as-cast $(Cu_{47.5}Zr_{47.5}Al_5)_{100-x}V_x$ (x=0, 1, 3, 5 and 10) samples at room temperature. Representative engineering stress–strain curves for these samples are shown in Fig. 5 and the mechanical properties are summarized in Table 3. For easy observation, each stress–strain curve is shifted relatively to the right by 0.01 strain. Only $Cu_{47.5}Zr_{47.5}Al_5$ and $(Cu_{47.5}Zr_{47.5}Al_5)_{99}V_1$ alloys exhibit notable compressive plasticity and, specifically, the fracture strains are 4.7% and 9.4%, respectively. Both alloys have the yield strength of about 1.85 GPa. In contrast, $(Cu_{47.5}Zr_{47.5}Al_5)_{95}V_5$ and $(Cu_{47.5}Zr_{47.5}Al_5)_{90}V_{10}$ samples fail catastrophically even before yielding, exhibit no plasticity. The compressive fracture strengths are 1.31 and 1.07 GPa for the 5 at% and 10 at% V-containing alloys, respectively. The intermediate alloy, $(Cu_{47.5}Zr_{47.5}Al_5)_{97}V_3$, fails also in the elastic region but still can reach a full yield strength of 1.85 GPa. It is apparent that, when V content is over about 1 at%, brittle V-rich intermetallic compound phases ($V+Al_{23}V_4$) begin to form and, subsequently, cause a detrimental effect on plasticity.

The plastic region in the stress–strain curves of $Cu_{47.5}Zr_{47.5}Al_5$ and $(Cu_{47.5}Zr_{47.5}Al_5)_{99}V_1$ is serrated, similar to other metallic glasses exhibiting compressive strain, and each serration

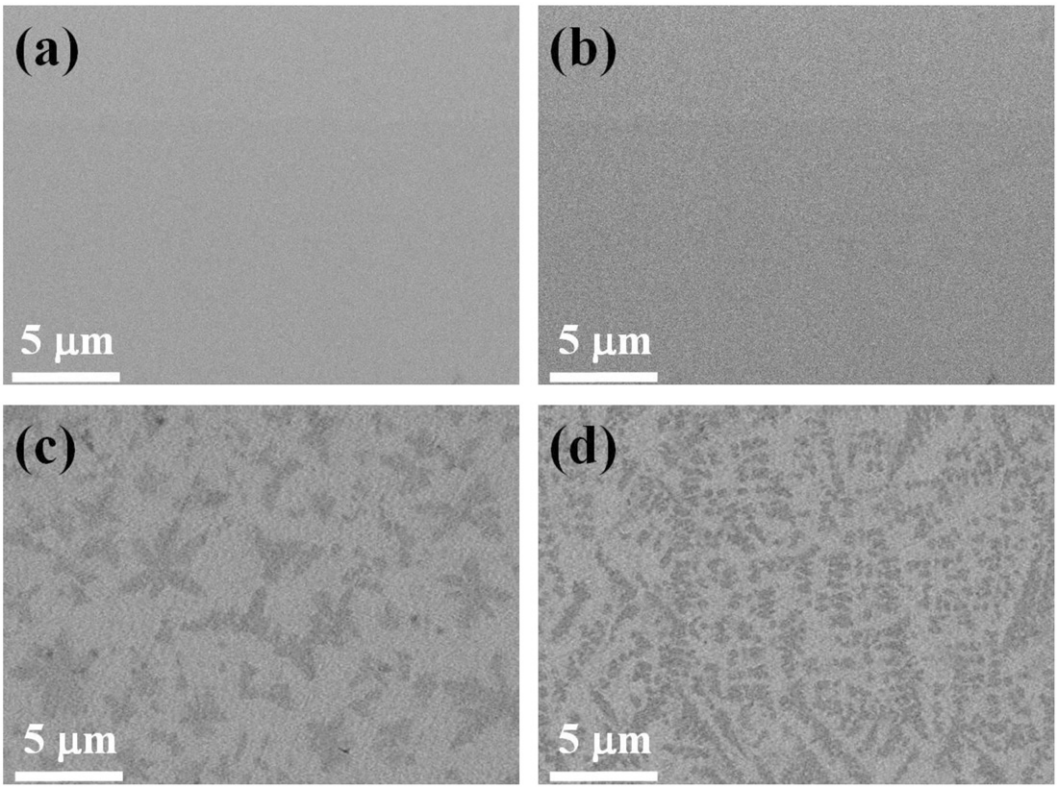

Fig. 3. SEM micrographs showing the as cast microstructures: (a) $Cu_{47.5}Zr_{47.5}Al_5$, (b) $(Cu_{47.5}Zr_{47.5}Al_5)_{99}V_1$, (c) $(Cu_{47.5}Zr_{47.5}Al_5)_{97}V_3$, and $(Cu_{47.5}Zr_{47.5}Al_5)_{90}V_{10}$. The dendritic gray phases are the V-containing phases (including pure V and $Al_{23}V_4$).

corresponds to the propagation of one shear band [8,19]. The total numbers of serration to failure are counted to be 113 and 259 for $Cu_{47.5}Zr_{47.5}Al_5$ and $(Cu_{47.5}Zr_{47.5}Al_5)_{99}V_1$, who fracture at 4.7% and 9.4%, respectively. There is no obvious difference in the number of shear bands per unit strain (~35 shear bands per 1% strain) in these two samples. Special effort was also made to estimate the amplitude of stress serrations in Fig. 5. The serration amplitude was 0.0126 GPa in $Cu_{47.5}Zr_{47.5}Al_5$ and only slightly higher (0.0159 GPa) in $(Cu_{47.5}Zr_{47.5}Al_5)_{99}V_1$; the average stress serrations are also similar. It is pointed out that the first discernible strain burst (marked on the curves in Fig. 5) is associated with shear band formation. It occurs at 1.47 GPa in $Cu_{47.5}Zr_{47.5}Al_5$ and at a slightly lower value of 1.35 GPa in $(Cu_{47.5}Zr_{47.5}Al_5)_{99}V_1$. These stresses correspond to 0.78 and $0.73\sigma_y$, where σ_y is the "macroscopic" yield strength of the alloy, i.e. the stress plateau in the plastic region. The ratios are in good agreement with that reported in other BMG alloys (~$0.79\sigma_y$) [20–22].

4. Discussion

Aghamiry et al. [15] point out that the minor addition of V would encourage the precipitation of Cu–Zr phase. Meanwhile, the strength reach its maximum at 1 at% V, and the plasticity is enhanced to 0.7% with 2 at% V addition due to the interaction of crystalline phases with shear bands which leads high density and extended distribution of shear bands. Our results also show the similar trend, while the optimum plasticity occurs at 1 at% V. The minor difference might be a result of minor composition difference. In addition, the glass forming ability of BMGs was seen to decrease with higher V contents with intermetallic particles being precipitated [15]. In comparison, our works also found the $Al_{23}V_4$ intermetallic second phase.

The data presented so far indicate that the addition of 1 at% V to $Cu_{47.5}Zr_{47.5}Al_5$ improves the compressive plasticity but higher V addition degrades the plasticity. The fact that the serration density, i.e. shear band numbers per unit strain, is essentially the same in both $Cu_{47.5}Zr_{47.5}Al_5$ and $(Cu_{47.5}Zr_{47.5}Al_5)_{99}V_1$ (Fig. 5) suggests that the observed plasticity enhancement in $(Cu_{47.5}Zr_{47.5}Al_5)_{99}V_1$ is not a result of shear-band multiplication, as often reported in BMGs with improved plasticity [23]. The amplitude of stress serration is associated with energy dissipation during shear band propagation. Our data indicate that the serration amplitude in the two alloys is comparable (0.0126 GPa versus 0.0159 GPa) suggesting that the energy dissipated during shear band propagation in the two alloys is also similar. In other words, the presence of V appears to have insignificant effect on the energy dissipation during plastic deformation.

Strain burst on a stress–strain curve is associated with shear band formation [19]. The first discernible burst is considered the very onset of yielding and is affected by the initial free volume content in a BMG alloy [24,25]. The result that $(Cu_{47.5}Zr_{47.5}Al_5)_{99}V_1$ has a lower strength (1.35 GPa) than that of $Cu_{47.5}Zr_{47.5}Al_5$ (1.47 GPa) suggests that the 1 at% V addition might have higher free volume content. However, according to

Table 2
Summary of the volume fractions in various specimens under the as-cast and after deformed conditions. The volume fraction for the as-cast $Cu_{47.5}Zr_{47.5}Al_5$ is quite low, difficult to be calculated to a precise value, thus shown as $<0.5\%$ in the table.

Specimen	As cast		After deformed	
	B2 ZrCu	V-containing phase	B2 ZrCu	V-containing phase
$Cu_{47.5}Zr_{47.5}Al_5$	$<0.5\%$	0	$1.5\pm0.2\%$	0
$(Cu_{47.5}Zr_{47.5}Al_5)_{99}V_1$	$1\pm0.3\%$	0	$7.2\pm1\%$	0
$(Cu_{47.5}Zr_{47.5}Al_5)_{97}V_3$	–	~8%	–	–
$(Cu_{47.5}Zr_{47.5}Al_5)_{95}V_5$	–	~10%	–	–
$(Cu_{47.5}Zr_{47.5}Al_5)_{90}V_{10}$	–	~15%	–	–

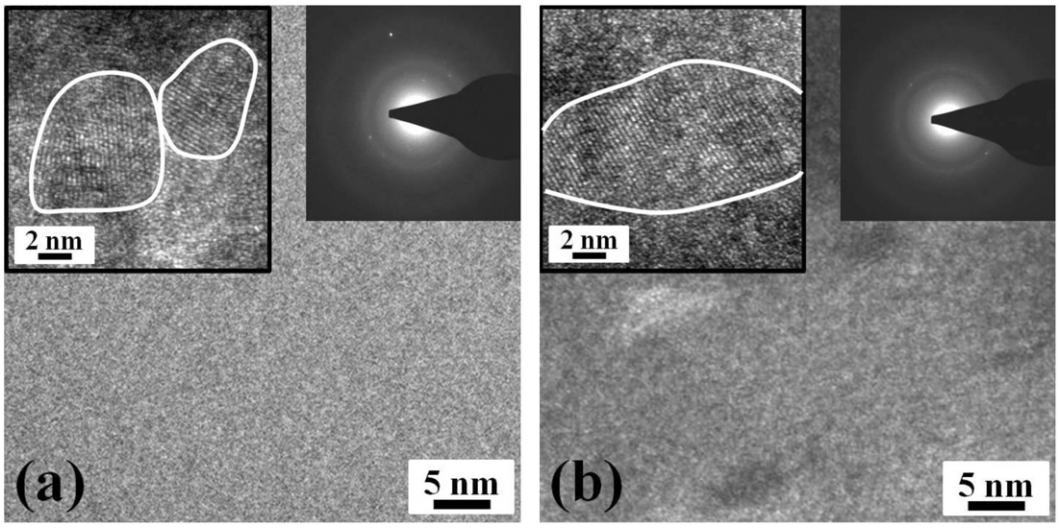

Fig. 4. TEM bright field images with the inserted high resolution images and associated diffraction patterns for (a) the deformed $Cu_{47.5}Zr_{47.5}Al_5$ sample, and (b) the deformed $(Cu_{47.5}Zr_{47.5}Al_5)_{99}V_1$ sample. The few fine nano B2 phase is not apparent in the diffraction pattern, but can be clearly seen in high resolution micrographs where the fine B2 CuZr precipitates are imbedded in the amorphous matrix.

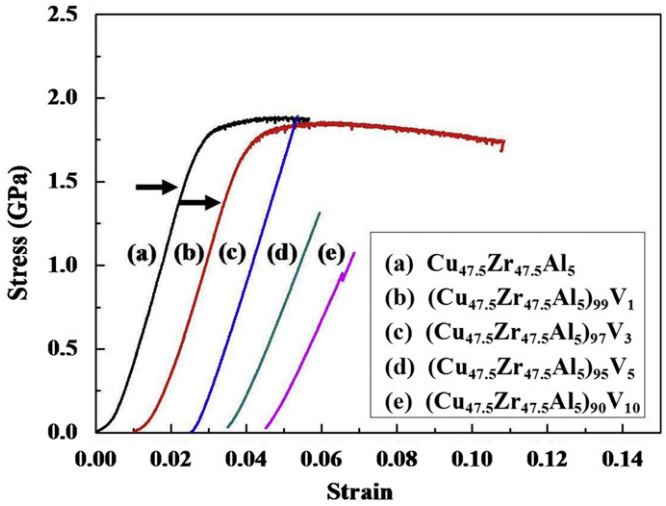

Fig. 5. Engineering stress and strain curves for the five alloys studied. Each curve is shifted to the right by 0.01 strain for easy comparison.

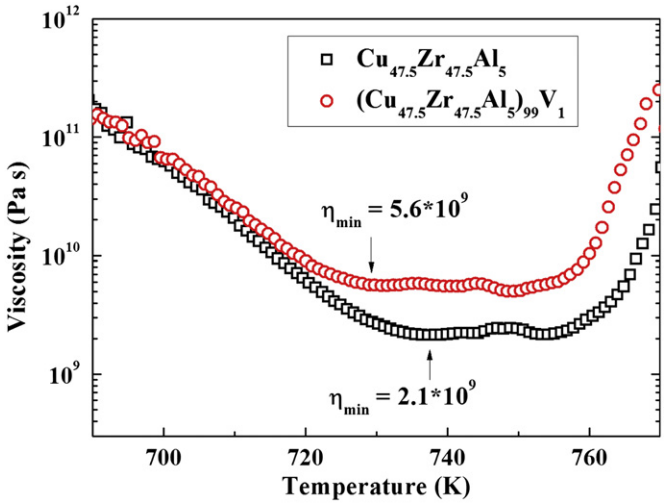

Fig. 6. Variation of viscosity (measured by TMA) as a function temperature for the $Cu_{47.5}Zr_{47.5}Al_5$ and $(Cu_{47.5}Zr_{47.5}Al_5)_{99}V_1$ alloys.

Table 3
Summary of mechanical properties of the as-cast Cu-based BMG at a strain rate of $1\times10^{-4}\ s^{-1}$ at room temperature.

Specimen	E (GPa)	σ_y (GPa)	ε_e (%)	ε_p (%)	ε_t (%)
$Cu_{47.5}Zr_{47.5}Al_5$	90	1.88	2.0	2.7	4.7
$(Cu_{47.5}Zr_{47.5}Al_5)_{99}V_1$	90	1.85	2.0	7.4	9.4
$(Cu_{47.5}Zr_{47.5}Al_5)_{97}V_3$	90	1.89	2.0	0	2.0
$(Cu_{47.5}Zr_{47.5}Al_5)_{95}V_5$	88	1.31	1.4	0	1.4
$(Cu_{47.5}Zr_{47.5}Al_5)_{90}V_{10}$	86	1.07	1.3	0	1.3

Spaepen's constitutive equation and related deviation [24], the yield strength was found to be extremely sensitive to the free volume content. It follows that such a small change in strength is unlikely to be caused by an appreciable change in free volume. Thus, the observed improved plasticity is unlikely resulted from significant increase in free volume caused by the V addition, either.

As mentioned before, the addition of V to the $Cu_{47.5}Zr_{47.5}Al_5$ alloy could cause the melt to separate into the Cu-rich and V-rich regions during casting because a positive heat of mixing between Cu and V. To demonstrate the effect of V on the phase separation, TMA was conducted to measure the viscosity of $Cu_{47.5}Zr_{47.5}Al_5$ and $(Cu_{47.5}Zr_{47.5}Al_5)_{99}V_1$ as a function of temperature and the results are given in Fig. 6. It is noted that, in the supercooled liquid region, $(Cu_{47.5}Zr_{47.5}Al_5)_{99}V_1$ BMG sample exhibits a minimum viscosity (η_{min}) of $\sim6\times10^9$ Pa s, which is higher than $\sim2\times10^9$ Pa s for $Cu_{47.5}Zr_{47.5}Al_5$. It is a three-fold increase in viscosity by adding 1 at% V into the $Cu_{47.5}Zr_{47.5}Al_5$. This increase is consistent with the notion that a composite (nanocrystals dispersed in a glass matrix) is usually more viscous than its monolithic counterpart. Thus, the TMA result supports the idea that the addition of V to $Cu_{47.5}Zr_{47.5}Al_5$ causes phase separation.

When V concentration is high (> 1 at%), however, intermetallic $Al_{23}V_4$ is formed (see Fig. 3). It suggests that V has a higher affinity to Al than to Cu or Zr. In other words, V and Al atoms tend to agglomerate or cluster in the glass matrix and form $Al_{23}V_4$ when the V concentration is excessive (> 1%), as indicated in Table 2. Intermetallic particles are usually brittle, especially when their sizes are larger than ~1 μm. In the current case, the dimension of $Al_{23}V_4$ is about 1–5 μm. Upon loading, $Al_{23}V_4$ is weaker than the strong amorphous matrix, thus fractures first whilst the amorphous matrix is still in the elastic range.

The fractured $Al_{23}V_4$ subsequently becomes shear band initiation site and exacerbates the fracture process.

When V content is low, for example, in the $(Cu_{47.5}Zr_{47.5}Al_5)_{99}V_1$ alloy, no V-containing compound could be found in the sample. Since V is practically insoluble in Al [17], Cu and Zr constituents in the alloy apparently open up the Al–V solid-solution phase field. Also, since the heat of mixing of Cu–Zr and V–Al is more negative than that of Cu–Al and V–Zr, it results in the formation of the Cu–Zr rich and V–Al rich regions, i.e. the depletion of Al from the original Cu–Zr–Al matrix. Aluminum depletion produces an amorphous matrix with a higher Cu–Zr content and, thus, thermodynamically favors the formation of B2-CuZr particles during cooling. In fact, the composition of the amorphous matrix is close to equimolar Cu–Zr.

Pauly et al. [12] pointed out that the presence of fine B2-CuZr could enhance plasticity and prevent catastrophic failure in $Cu_{47.5}Zr_{47.5}Al_5$. The B2 particles greater than about 25 nm appeared to have undergone twinning transformation. The microstructure of the current V-containing alloy was examined using TEM. Bright-field and high-resolution TEM micrographs taken from deformed $Cu_{47.5}Zr_{47.5}Al_5$ and $(Cu_{47.5}Zr_{47.5}Al_5)_{99}V_1$ are given in Figs. 4(b) and (d), which show the dispersion of nanocrystals in the amorphous matrix. Through the determination of the lattice constant by fast Fourier transformation (FFT) filter of the ordered regions, the nanocrystals in both samples are identified to be B2 CuZr, as shown in Figs. 4(b) and (d). No nanocrystal was discernible in the as-cast $Cu_{47.5}Zr_{47.5}Al_5$, but a slight amount of nanocrystals was observed in the deformed sample. Both the density and size of the B2 phase in the deformed $Cu_{47.5}Zr_{47.5}Al_5$ and $(Cu_{47.5}Zr_{47.5}Al_5)_{99}V_1$ are much higher than that in the as-cast specimens, as indicated in Table 2. In addition, more and larger B2 nanocrystals are observed in the deformed $(Cu_{47.5}Zr_{47.5}Al_5)_{99}V_1$ sample (~7.2 vol% and ~10 nm in diameter) as compared to that in the deformed $Cu_{47.5}Zr_{47.5}Al_5$ (~1.5 vol% and ~5 nm in diameter). It is evident that deformation can induce precipitate growth in the current BMGs, consistent with the previous observation [12]. Twinning and phase transformation in B2-CuZr have been suggested to contribute to the ductility improvement in CuZrAl-based metallic glasses [12,13]. However, in the current study, no twin formation or phase transformation of the current fine B2-particles (all less than 10 nm) was observed in the $(Cu_{47.5}Zr_{47.5}Al_5)_{99}V_1$ alloy, excluding the possibility that twinning or phase transformation has contributed to the observed plasticity enhancement. A plausible explanation might be related to the size of B2 particles. When the B2 particles are measured greater than ~25 nm, the accumulated shear stress within the B2 phase is high enough to induce twinning or even martensitic transformation. But if the B2 phase is too small, as in the range of 10 nm or less, twinning or martensitic transformation would not be able to proceed. There seems to be a critical size for the induction of twinning or martensitic transformation.

Pauly et al. [12] suggested that deformation-induced growth of B2-CuZr could dissipate energy, prevent catastrophic shear band propagation and, thus, improve plasticity. In the current $(Cu_{47.5}Zr_{47.5}Al_5)_{99}V_1$ sample, the mean size of B2 particles increases from the initial 3–5 nm to 10 nm, and the volume fraction also increases from 0.8 vol% to 7.2 vol% after deformation. However, the number of B2 particles in the sample is noted to decrease after deformation; specifically, they are $12^*10^4/m^3$ and $8.4^*10^4/m^3$ in samples before and after deformation. The reduction of particle number indicates that some small CuZr particles were dissolved during plastic deformation. The observation is also consistent with the fact that volume fraction of the B2 phase increases from 0.8 vol% to only 7.2 vol%; the volume fraction is evaluated to be 12.5% if all initial particles grow simultaneously. It further suggests that the nucleation of new B2 particle during deformation was negligible. In the following, we perform an analysis to elucidate the energy balance during deformation.

The initial and final energy densities of the system, as illustrated in Fig. 7, are

$$n_0(4\pi r_0^3/3)G_p + n_0(4\pi r_0^2)\gamma_{p-m} + (1-f_0)G_m, \tag{2}$$

and

$$n_1(4\pi r_1^3/3)G_p + n_1(4\pi r_1^2)\gamma_{p-m} + (1-f_1)G_m, \tag{3}$$

where the subscripts 0 and 1 represent the initial and final states, respectively. In the expressions, G_p and G_m are the energy density of the particle and matrix, r is the average diameters of the B2 particle, n is the number density per unit volume of the B2 particles, and γ_{p-m} is the particle–matrix interface energy, and $f(=n(4\pi r^3/3))$ is the volume fractions of the B2 particle. Assuming there is no heat loss, energy balance would require the mechanical work (W) done to be

$$W = (f_1 - f_0)(G_p - G_m) + 3\gamma_{p-m}\left(\frac{f_1}{r_1} - \frac{f_0}{r_0}\right) \tag{4}$$

In the equation, $(G_p - G_m)$ is essentially the crystallization energy, which is estimated to be 2.21^*10^9 J/m^3 from previous DSC measurements [26,27]. Substitute data from the current measurements, we obtain $\gamma_{p-m}=0.293$ J/m^2 as the particle–matrix interface energy in the $(Cu_{47.5}Zr_{47.5}Al_5)_{99}V_1$ sample. To our best knowledge, there is no experimental datum for the crystallized particle–amorphous matrix interface energy in any

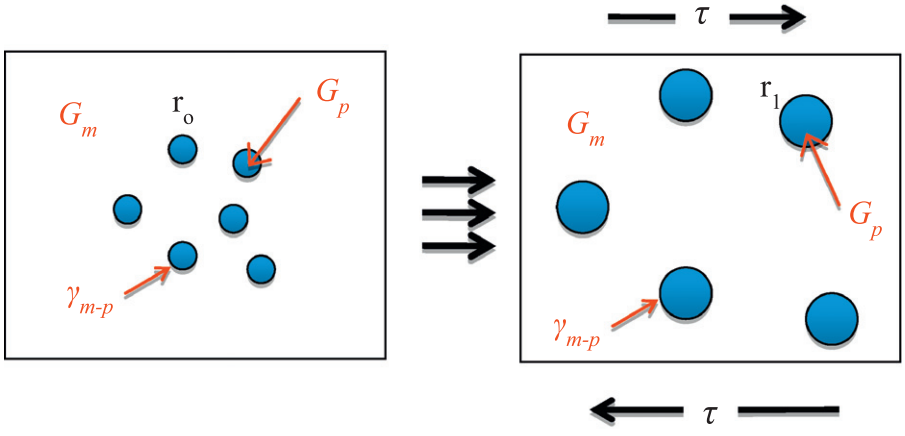

Fig. 7. The initial and final energy densities of the system.

metallic glass system, although it was expected to be low [28]. The only available datum is for silicon, which is about 0.4 J/m^2 [29]. In comparison, the crystalline–crystalline interface energy, for example, the θ' precipitate–aluminum interface is about 1.5 J/m^2 [30]. The current estimation of γ_{p-m} for B2-CuZr appears to be in the right range.

Since the interface energy is directly related to the coarsening, within the classical coarsening theory [31], the above reasonable extracted interface energy implies that the coarsening argument is logical. From the energy point of view, our current results appear to indirectly support the idea of Pauly et al. [12], i.e. plasticity improvement in $(Cu_{47.5}Zr_{47.5}Al_5)_{99}V_1$ is attributable to the dynamic coarsening of B2-CuZr particles, when the B2 particles are too small to induce twinning or martensitic transformation. The fine B2 particles in the current alloys appear to be unstable, and would undergo coarsening during deformation. It is expected that once the B2 particles grow larger to a level of a few tens of nanometers, twinning or martensitic transformation might be induced.

5. Conclusions

A series of $(Cu_{47.5}Zr_{47.5}Al_5)_{100-x}V_x$ (x=0, 1, 2, 3, 5, and 10) (in at%) alloys were synthesized and tested in compression. Microstructural examination showed that V was dissolved in the amorphous matrix and promoted the formation of B2-CuZr precipitates in $(Cu_{47.5}Zr_{47.5}Al_5)_{99}V_1$. However, when V content is more than 3 at%, brittle intermetallic compound phases ($V+Al_{23}V_4$) form and degrade the plasticity. Specifically, compressive plasticity in all $(Cu_{47.5}Zr_{47.5}Al_5)_{100-x}V_x$ alloys is practically nil, except in alloys that with x=1 or 0. Plasticity improvement was observed only in the $(Cu_{47.5}Zr_{47.5}Al_5)_{99}V_1$ alloy and, specifically, fracture strain doubles from 4.7% to 9.4%. Shear-band multiplication, energy dissipation by viscous flow serration, mechanical twinning and deformation-induced phase transformation of B2-CuZr particles were excluded as the possible mechanism for the current fine B2 particles measuring 3–5 nm. An energy-balance analysis based on deformation-induced B2 particle coarsening produced an interfacial energy of 0.293 J/m^2 for the B2 particle–glassy matrix interface. This energy value agrees with the available amorphous–crystal interface energy in the literature for silicon, which is about 0.4 J/m^2. The result appears to indirectly support the idea suggested by Pauly et al. [12] that plasticity in $Cu_{47.5}Zr_{47.5}Al_5$ is caused by dynamic coarsening of the B2-CuZr particles. It is expected that once the B2 particles grow larger to a level of a few tens of nanometers, twinning or martensitic transformation might be induced.

Acknowledgments

The authors gratefully acknowledge the sponsorship from National Science Council of Taiwan, ROC, under the project no. NSC 98-2221-E-110-036-MY3. T.G.N. is supported by the National Science Foundation under Contract DMR-0905979.

References

[1] W.L. Johnson, MRS Bull. 24 (1999) 42–56.
[2] A. Inoue, Acta Mater. 48 (2000) 279–306.
[3] W.H. Wang, C. Dong, C.H. Shek, Mater. Sci. Eng. R-Rep. 44 (2004) 45–89.
[4] J.C. Huang, J.P. Chu, J.S.C. Jang, Intermetallics 17 (2009) 973–987.
[5] C.A. Pampillo, J. Mater. Sci. 10 (1975) 1194–1227.
[6] C.T. Liu, L. Heatherly, D.S. Easton, C.A. Carmichael, J.H. Schneibel, C.H. Chen, J.L. Wright, M.H. Yoo, J.A. Horton, A. Inoue, Metall. Mater. Trans. A29 (1998) 1811–1820.
[7] C.A. Schuh, T.C. Hufnagel, U. Ramamurty, Acta Mater. 55 (2007) 4067–4109.
[8] S.X. Song, H. Bei, J. Wadsworth, T.G. Nieh, Intermetallics 16 (2008) 813–818.
[9] H.M. Chen, X.H. Du, J.C. Huang, J.S.C. Jang, T.G. Nieh, Intermetallics 17 (2009) 330–335.
[10] R.D. Conner, R.B. Dandliker, W.L. Johnson, Acta Mater. 46 (1998) 6089–6102.
[11] C.C. Hays, C.P. Kim, W.L. Johnson, Phys. Rev. Lett. 84 (2000) 2901–2904.
[12] S. Pauly, S. Gorantla, G. Wang, U. Kühn, a.J. Eckert, Nat. Mater. 9 (2010) 473–477.
[13] Y. Wu, Y. Xiao, G. Chen, C.T. Liu, Z. Lu, Adv. Mater. 22 (2010) 2770–2773.
[14] A. Takeuchi, A. Inoue, Mater. Trans. JIM 41 (2000) 1372–1378.
[15] E. Aghamiry, R. Gholampour, N. Khademian, Mater. Sci. Eng., A 547 (2012) 80–85.
[16] X.Y. Lu, M. Kolbe, D.M. Herlach, Mater. Res. Soc. 754 (2003) 21–26.
[17] S. Nagasaki, M. Hirabayashi, Binary Alloy Phase Diagrams, Metallurgical Industry Press, Beijing, China, 2004.
[18] J. Gurland, Quantitative Microscopy, McGraw-Hill, 1968.
[19] W.J. Wright, R. Saha, W.D. Nix, Mater. Trans. JIM 42 (2001) 642–649.
[20] S.X. Song, T.G. Nieh, Intermetallics 17 (2009) 762–767.
[21] S.X. Song, X.-L. Wang, T.G. Nieh, Scr. Mater. 62 (2010) 847–850.
[22] C.N. Kuo, H.M. Chen, X.H. Du, J.C. Huang, Intermetallics 18 (2010) 1648–1652.
[23] Y.H. Liu, G. Wang, R.J. Wang, D.Q. Zhao, M.X. Pan, W.H. Wang, Science 315 (2007) 1385–1388.
[24] J.G. Wang, D.Q. Zhao, M.X. Pan, W.H. Wang, S.X. Song, T.G. Nieh, Scr. Mater. 62 (2010) 477–480.
[25] L. Wang, H. Bei, Y.F. Gao, Z.P. Lu, T.G. Nieh, Acta Mater. 59 (2011) 7627–7633.
[26] D. Xu, B. Lohwongwatana, G. Duan, W.L. Johnson, C. Garland, Acta Mater. 52 (2004) 2621–2624.
[27] M.B. Tang, D.Q. Zhao, M.X. Pan, W.H. Wang, Chin. Phys. Lett. 21 (2004) 901–903.
[28] A. Hirata, Y. Hirotsu, E. Matsubara, T. Ohkubo, K. Hono, Phys. Rev. B 74 (2006) 184204.
[29] N. Bernstein, M.J. Aziz, E. Kaxiras, Phys. Rev. B 58 (1998) 4579–4583.
[30] J.D. Boyd, R.B. Nicholson, Acta Mater. 19 (1971) 1101–1109.
[31] J. Christian, The Theory of Transformation in Metals and Alloys, second ed., Pergamon Press, Oxford, 1975.